Supplementary Material: Changes in temperature and rainfall extremes across East Asia in the CMIP5 ensemble

Youngsaeng Lee[1,3] Jayeong Paek[2,3] Jeong-Soo Park[3,*]
Kyung-On Boo[4]

1: Digital Transformation Department, Korea Electric Power Corporation, Korea
2: Institute for Biomedical Science, Chonnam National University Hwasun Hospital, Korea
3: Department of Statistics, Chonnam National University, Gwangju 500-757, Korea
4: Korea Meteorological Administration, Korea
**: Corresponding author, E-mail: jspark@jnu.ac.kr, Tel: +82-62-530-3445*

Feb 2020

1 Datasets

We used the same dataset as in Kharin et al (2013) (hereafter referred to as K13), by following their approach. CMIP5 models analyzed in this study are listed in Table S1 together with the spatial resolutions of their atmospheric components. The number of ensemble simulations for each model and experiment is listed in Table S2. Output from 32 CMIP5 models was available for the historical experiment, from 22 codes for the RCP2.6 experiment, 31 models for the RCP4.5 experiment (not all years for some models), and 31 codes for the RCP8.5 experiment. The list of these tables are same to the tables in Supplementary Material of K13.

Observationally-based (or reanalysis) datasets used for the evaluation of temperature and rainfall extremes in the historical record are listed in Table S3. The used four reanalysis are the National Centers for Environmental Prediction-National Center for Atmospheric Research (NCEP-NCAR) reanalysis (Kalnay et al 1996) denoted hereafter as NCEP1, the European Centre for Medium-Range Weather Forecasts (ECMWF) ERA40 reanalysis (Uppala et al 2005), the NCEP-Department of Energy AMIP-II reanalysis (Kanamitsu et al 2002) denoted as NCEP2, and ECMWF ERA-Interim reanalysis (Dee et al 2011) denoted as ERA-I. Model-simulated extremes of non-overlapping 5-day rainfall rates (pentads) are also verified against the Climate Prediction Center Merged Analysis of Precipitation (CMAP) pentad dataset from the NCEP-

NCAR reanalysis (Xie and Arkin 1997), and the experimental global precipitation (GPCP) pentad dataset (Xie et al 2003).

2 Methodology

For the methods of data analysis, we follow the approach of Kharin et al (2013) and the references therein for analysis of climate extremes of near surface air temperature and daily rainfall amounts. For this purpose, we use a generalized extreme value (GEV) distribution that is fitted at every grid point to samples of annual temperature and rainfall extremes.

The GEVD is widely used to analyse univariate extreme values. The three types of extreme value distributions are sub-classes of GEVD. The cumulative distribution function of the GEVD is as follows:

$$G(x) = exp\left\{-\left(1+\xi\frac{x-\mu}{\sigma}\right)^{-1/\xi}\right\}, \tag{1}$$

when $1+\xi(x-\mu)/\sigma > 0$, where μ, σ, and ξ are the location, scale, and shape parameters, respectively. The particular case for $\xi = 0$ in Eq. (1) is the Gumbel distribution, whereas the cases for $\xi > 0$ and $\xi < 0$ are known as the Fréchet and the negative Weibull distributions, respectively (Coles, 2001).

Assuming the data, the annual maxima of daily rainfall in this study, follow (approximately) a GEV distribution, the parameters can be estimated by using the maximum likelihood method (e.g., Coles 2001) or the method of L-moments estimation. The maximum likelihood estimator is less efficient than the L-moments estimator in small samples for typical shape parameter values (Hosking 1990). The L-moments method is used in this study because relatively short 30-year samples are analyzed for each comparison period. Moreover, the formulae used to obtain the L-moments estimator are simple compared with obtaining the maximum likelihood estimator which needs an iterative computation until convergence. The L-moments estimator are

$$\hat{\xi} = 7.8590c + 2.9554c^2 \tag{2}$$

where

$$c = \frac{2l_2}{l_3+3l_2} - \frac{ln(2)}{ln(3)}, \tag{3}$$

and l_2 and l_3 are the sample second and third L-moments (Hosking, 1990). The other parameters are then given by

$$\sigma = \frac{\hat{\xi}\, l_2}{\Gamma(1+\hat{\xi})\,(1-2^{-\hat{\xi}})} \tag{4}$$

$$\mu = l_1 + \frac{\hat{\sigma}[\Gamma(1+\hat{\xi})-1]}{\hat{\xi}}, \tag{5}$$

Table S 1: The list of CMIP5 climate models analyzed in the present study and their horizontal and vertical resolutions. Model resolution is characterized by the size of a horizontal grid on which output is available from the model's atmospheric component and by the number of vertical levels. Spectral models are also characterized by their spectral truncations in brackets.

Model	Institution	Resolution (Lon x Lat x Level #)
ACCESS1-0	Commonwealth Scientific & Industrial Research Organization/Bureau of Meteo., Australia	192×145L38
bcc-csm1-1	Beijing Climate Center, China Meteo. Admin.	128×64L26(T42)
bcc-csm1-1-m	Beijing Climate Center, China Meteo. Admin.	320×160
BNU-ESM	Beijing Normal University, China	128×64L26(T42)
CanESM2	Canadian Centre for Climate Modelling & Analysis	128×64L35(T63)
CCSM4	National Center for Atmospheric Research, USA	288×192L26
CMCC-CM	Centro Euro-Mediterraneo per I Cambiamenti, Italy	480×240L31(T159)
CMCC-CMS	Centro Euro-Mediterraneo per I Cambiamenti, Italy	192×96
CNRM-CM5	Centre National de Recherches Meteorologiques, Meteo-France	256×128L31(T127)
CSIRO-Mk3-6-0	Australian Commonwealth Scientific & Industrial Research Organization	192×96L18(T63)
FGOALS-g2	Inst. Atmospheric Physics, Chinese Academy of Sciences, Tsinghua University	128×60L26
FGOALS-s2	Inst. Atmospheric Physics, Chinese Academy of Sciences	128×108L26
GFDL-CM3	Geophysical Fluid Dynamics Laboratory, USA	144×90L48
GFDL-ESM2G	Geophysical Fluid Dynamics Laboratory, USA	144×90L24
GFDL-ESM2M	Geophysical Fluid Dynamics Laboratory, USA	144×90L24
HadGEM2-AO	UK Met Office Hadley Centre	96×73L19
HadGEM2-CC	UK Met Office Hadley Centre	192×145L40
HadGEM2-ES	UK Met Office Hadley Centre	192×145L40
inmcm4	Institute for Numerical Mathematics, Russia	180×120L21
IPSL-CM5A-LR	Inst. Pierre-Simon Laplace, France	96×96L39
IPSL-CM5A-MR	Inst. Pierre-Simon Laplace, France	144×143L39
IPSL-CM5B-LR	Inst. Pierre-Simon Laplace, France	96×96L39
MIROC5	Model for Interdisciplinary Research on Climate, Japan	256×128L40(T85)
MIROC-ESM	Model for Interdisciplinary Research on Climate, Japan	128×64L80(T42)
MIROC-ESM-CHEM	Model for Interdisciplinary Research on Climate, Japan	128×64L80(T42)
MPI-ESM-LR	Max Planck Institute for Meteorology, Germany	192×96L47(T63)
MPI-ESM-MR	Max Planck Institute for Meteorology, Germany	192×96L95(T63)
MRI-CGCM3	Meteorological Research Institute, Japan	320×160L48(T159)
NorESM1-M	Norwegian Climate Centre	144×96L26

Table S 2: The rainfall simulation codes used in this study are listed. The symbol and number in blanket are for temperature numerical models. Model output is generally available for year 1850-2005 for the historical experiment, and for years 2006-2100 for the RCP experiments.

Model	Historical	RCP2.6	RCP4.5	RCP8.5
ACCESS1-0	O	X	O	X
BCC-CSM1-1	O(X)	O(X)	O	O
BCC-CSM1-1-m	O	O	O	O
BNU-ESM	O(X)	O	O	O
CanESM2	O	O	O	O
CCSM4	O	O	O	O
CMCC-CM	O	X	O	X
CMCC-CMS	O	X	O	X
CNRM-CM5	O	O	O	O
CSIRO-Mk3-6-0	O	O	O	O
FGOALS-g2	O(X)	O(X)	O(X)	O(X)
FGOALS-s2	O	X	X	O(X)
GFDL-CM3	O	O	O	O
GFDL-ESM2G	O	O	O	O
GFDL-ESM2M	O	O	O	O
HadCM3-AO	O(X)	X	O(X)	O(X)
HadGEM2-CC	O	X	O	O
HadGEM2-ES	O	O	O	O
INMCM4	O	X	O	O
IPSL-CM5A-LR	O	O	O	O
IPSL-CM5A-MR	O	O	O	O
IPSL-CM5B-LR	O	X	O	X(O)
MIROC5	O	O	O	O
MIROC-ESM	O	O	O	O
MIROC-ESM-CHEM	O	O	O	O
MPI-ESM-LR	O	O	O	O
MPI-ESM-MR	O	O	O	O
MRI-CGCM3	O	O	O	O
NorESM1-M	O	O	O	O
Total #of models	29(25)	21(19)	28(26)	25 (23)

Table S 3: Reanalysis and observation-base datasets used in this study for validation of temperature and precipitation extremes.

Label	Grid size	Dataset and reference
ERA40	144x73	ECMWF ERA-40 reanalysis (Uppala et al., 2005)
ERA-I	240x121	ECMWF ERA-Interim reanalysis (Dee et al., 2011)
NCEP1	192x94	NCEP-NCAR reanalysis (Kalnay et al., 1996)
NCEP2	192x94	NCEP-DOE (Department Of Energy) AMIP-II reanalysis (Kanamitsu et al., 2002)
CMAP	144x72	Climate Prediction Center Merged Analysis of Precipitation (Xie and Arkin, 1997)
GPCP	144x72	Global Precipitation Climatology Project (Xie et al., 2003)

where l_1 is the first sample L-moment. The actual estimates are obtained with the feasibility modification of Dupuis and Tsao (1998).

When observations depend on time as a covariate, we employ the maximum likelihood method for estimating the parameters of a GEV distribution as in Coles (2001) or Kharin and Zwiers (2005). The parameters are estimated for each year from overlapping 51-year time windows. The location and scale parameters are assumed to depend linearly on time while the shape parameter is assumed to be time-invariant. An advantage of the maximum likelihood method is that time covariates can be included, which potentially allows extreme value statistics to be estimated more accurately for each individual year. In contrast, L-moment estimates are representative of a whole 20-year time slice (K13).

It can be helpful to describe changes in extremes in terms of changes in extreme quantiles. These are obtained by inverting (1):

$$z_p = \mu - \frac{\sigma}{\xi}[1 - \{-log(1-p)\}^{-\xi}], \tag{6}$$

where $G(z_p) = 1 - p$. Here, z_p is known as the return level associated with the waiting time (or return period) $1/p$, since the value z_p is expected to be exceeded on average once every $1/p$ years (Coles 2001). For example, a 20-year (50-year) return level is computed as the 95th (98th) percentile of the fitted GEVD. These return levels and waiting times are used as the main quantities in this study.

The projected changes in temperature and rainfall extremes are determined relative to the 1986-2005 reference period and are also expressed in terms of the corresponding changes in waiting times for climate extremes simulated in the reference period. The projected multimodel median changes are assessed with the Wilcoxon signed-rank test.

Following K13, we also estimate the dependence of local changes in extreme rainfall on mean temperature changes at the same location as simulated in the CMIP5 ensemble. This is done by fitting a GEV distribution to annual rainfall extremes at each grid point in the historical and all available RCP experiments for each model with the three GEV parameters linearly depending on mean temperature change at the same grid point. The resulting six parameters are estimated by the method of maximum likelihood. Once the parameters are estimated, the return levels and their changes per unit of warming are obtained by computing the corresponding quantiles of the GEV distribution (K13). For more technical details, readers are recommended to see the Supplementary Material of K13.

3 Simulated late 20th century climate extremes over East Asia

3.1 Evaluation of simulation models

Figure S1 shows the Taylor diagrams (Taylor 2001) of 29 CMIP5 models for the 20-year return levels of the largest daily rainfall (top left panel, R_{20}), coldest temperature (top right panel, TN_{20}), maximum 5-day precipitation (bottom left, R^5), and warmest temperature (bottom right panel, TX_{20}). The azimuthal angle represents the Pearson correlation coefficient (gray contours); the radial distance from the origin represents the normalized standard deviation of the scenario models and observations (blue dashed contours); and the distance from the point of observation on the x-axis represents the normalized root mean squared error (black dashed radial grid).

For the largest daily rainfall, the standard deviation (SD) of the observation (ERA-I) is 37.7mm, whereas those of the CMIP5 are distributed between 11.7mm and 70.2mm. The pattern correlations between the observation and multimodels are between 0.39 and 0.86, and the root mean squared errors (RMSEs) of the CMIP5 models are between 23.1mm and 36.2mm. For the maximum 5-day precipitation, the SD of ERA-I is 12.0mm, whereas those of the CMIP5 are between 5.0mm and 23mm. The pattern correlations are from 0.6 to 0.85, and the RMSEs of the models are between 7.5mm and 17mm. The CMIP5 models for the maximum 5-day precipitation have higher correlations to observations with less variations compared with those for the largest daily rainfall.

For the coldest temperature , the SD of the observation is 18.0°C, and those of the CMIP5 are between 13.4°C and 19.5°C. The correlations between ERA-I and the multimodels are between 0.94 and 0.97, and the RMSEs of the CMIP5 models are between 4.5°C and 8.5°C. Lastly, for the warmest temperature , the SD of the observation is 5.8°C, and those of the CMIP5 are between 3.4°C and 7.4°C. The correlations are between 0.76 and 0.89, and the RMSEs of the models are between 2.9°C and 5.1. The CMIP5 models for the coldest temper-

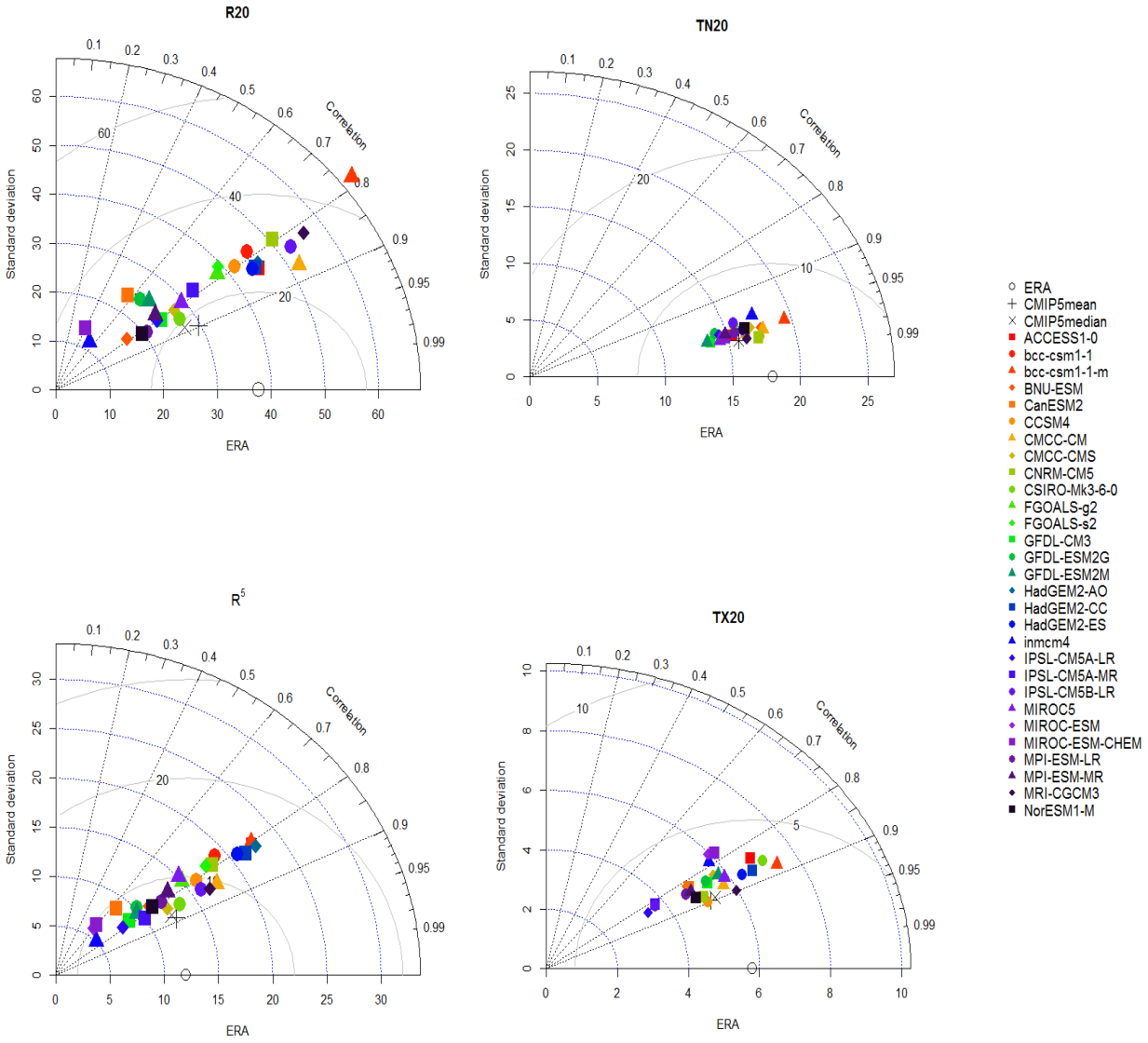

Figure S 1: Taylor diagrams for R_{20} (top left panel), TN_{20} (top right panel), R^5_{20} (bottom left panel), and TX_{20} (bottom right panel) are listed, where R_{20}, TN_{20}, R^5_{20}, and TX_{20} are 20-year return levels of 1986–2005 annual largest daily and 5-day rainfalls (mm), annual coldest and warmest temperatures (°C), respectively.

ature have higher correlations to the observations with more variations compared to those for the warmest temperature .

3.2 Reanalysis data and simulation models

The 20-year return levels of 1986-2005 annual warmest temperature and coldest temperature for the globe, East Asia, and Korea are summarized in Table S4. The quartiles of CMIP5 multimodel ensembles (MME) of 20-year return level in ERA-I and NCEP2 (Dee et al. 2011; Kanamitsu et al. 2002) are presented. Three quartiles of rainfall extremes for MME and median values from the reanalysis data are provided in Table S5. The return levels R_{20} and $\bar{R}^5_{20}$ obtained by CMIP5 MME for 1986-2005 over Korea, EA, and the globe are compared. These statistics are obtained by using the method of L-moments.

Table S 4: Three quartiles obtained from CMIP5 multimodel ensemble and the median from the reanalysis datasets for spatially averaged 20-year return levels of 1986-2005 annual warmest temperature (TX_{20}) and annual coldest temperature (TN_{20}).

	TX_{20} (°C)			TN_{20} (°C)		
Source	Globe	East Asia	Korea	Globe	East Asia	Korea
CMIP5 75%	26.60	32.41	32.00	0.20	-8.97	-5.87
CMIP5 50%	26.20	31.21	31.14	-0.80	-10.52	-7.55
CMIP5 25%	25.70	29.60	29.97	-1.40	-11.13	-8.89
ERA-I	25.60	30.74	30.77	0.10	-4.86	-4.00
NCEP2	26.40	31.49	32.73	-2.80	-7.92	-7.67

Figure S2 shows the zonally averaged 20-year return levels of 1986-2005 annual largest daily rainfall (R_{20}, top panel), the annual coldest temperature (TN, top right panel), non-overlapping 5-day mean rainfall ($\bar{R}^5_{20}$, middle left panel), and the annual warmest temperature (TX, middle right panel) as simulated by CMIP5 models plotted on a log scale. The CMAP and GPCP pentad rainfall extremes (Xie and Arkin 1997; Xie et al 2003) were used for obtaining $\bar{R}^5_{20}$. Note that the reanalysis datasets ERA40 and NCEP1 (Uppala et al 2005; Kalnay et al 1996) were also used in drawing this figure. In addition, box-and-whisker plots of regionally averaged statistics are provided, which are obtained from the reanalyses and CMAP and GPCP pentad datasets.

Figure S3 shows contour maps of 20-year return level of the annual largest daily rainfall for the reference period (1986–2005) obtained from four different reanalysis datasets (ERA-I,

Table S 5: Three quartiles obtained from CMIP5 multimodel ensemble and the median from the reanalysis datasets for spatially averaged 20-year return levels of annual largest daily rainfall (R_{20}) and for annual largest pentad precipitation ($\bar{R}^5_{20}$).

	R_{20} (mm/day)			$\bar{R}^5_{20}$ (mm/day)		
Source	Globe	East Asia	Korea	Globe	East Asia	Korea
CMIP5 75%	76.00	98.07	127.37	29.00	33.83	40.68
CMIP5 50%	65.00	80.02	108.60	26.00	29.50	36.25
CMIP5 25%	52.00	69.72	94.06	23.00	26.21	32.80
ERA-I	67.00	83.49	118.02	22.00	26.43	35.98
NCEP2	84.00	76.94	87.99	32.00	28.34	29.50
CMAP	-	-	-	24.00	29.26	44.11

ERA40, NCEP1, and NCEP2) across EA. Figure S4 is contour maps of 20-year return level of the annual maximum 5-day rainfall for the reference period obtained from 6 different reanalyses (ERA-I, ERA40, NCEP1, NCEP2, CMAP and GPCP). Figure S5 is contour plot of 20-year return level of the annual largest pentad precipitation obtained from CMIP5 ensemble for the historical data.

4 Projected future changes in climate extremes over East Asia

4.1 Changes in temperature extremes

Figure S6 shows contour maps of the future relative changes of the 20-year return levels in cold temperature extremes (TN_{20}) and in warm temperature extremes (TX_{20}) for 2081–2100 relative to 1986–2005 from the CMIP5 ensemble in the three RCP scenarios. Figure S7 displays the box-and-whisker plots of the future changes in temperature extremes as simulated by CMIP5 models in 2016-2035, 2046-2065, and 2081-2100 relative to 1986-2005.

In the Figures 3 and 4 in the paper, the changes of TN_{20} over EA by the end of 21st century are 1.9°C, 3.2°C, and 6.7°C for RCP2.6, RCP 4.5, and RCP 8.5 (0.9°C, 2.0°C, and 4.8°C for TX_{20}), respectively. These values over Korea are 1.3°C, 2.4°C, and 7.0°C for TN_{20}, and 1.6°C, 2.6°C, and 5.5°C for TX_{20}.

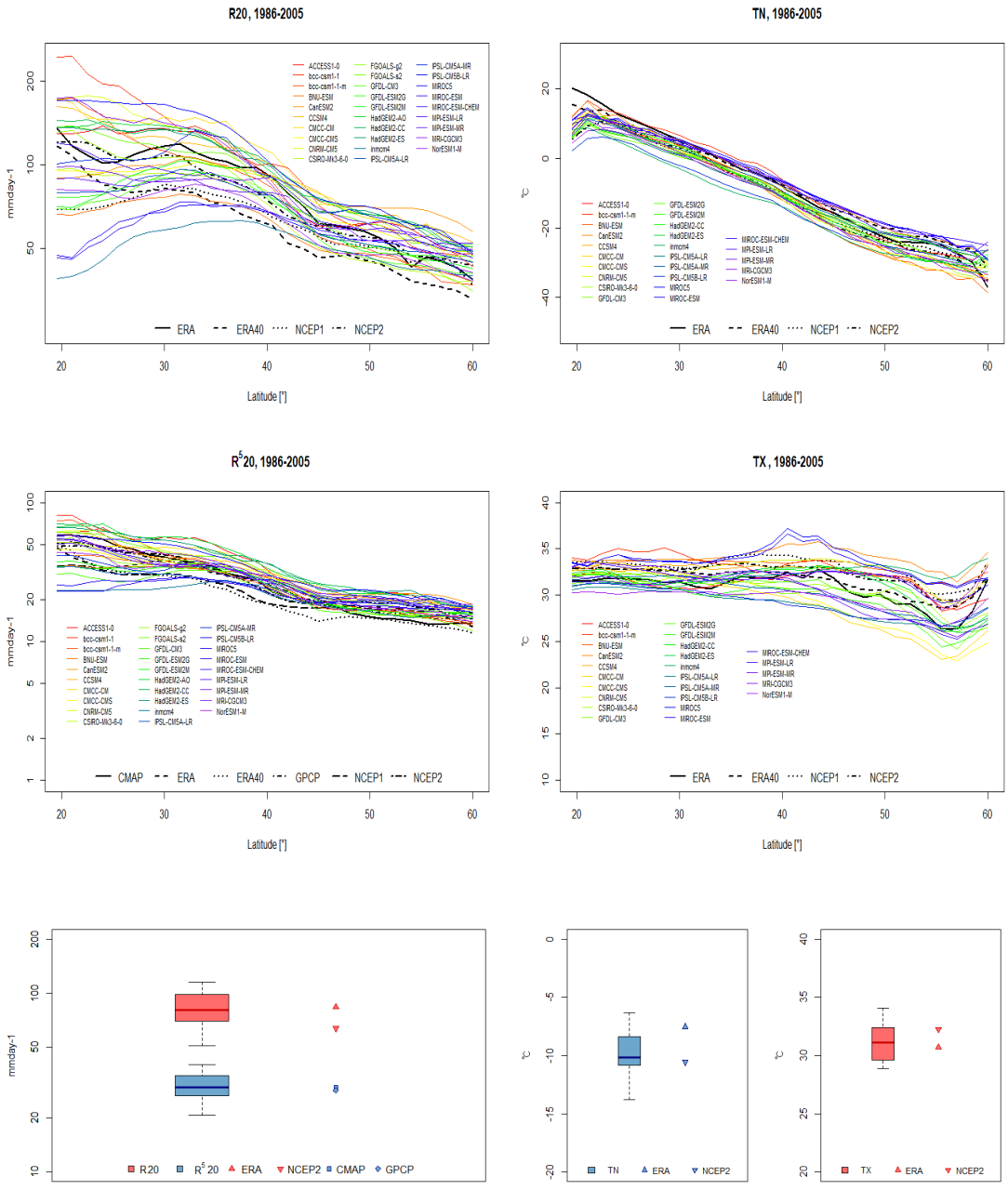

Figure S 2: Zonally averaged 20-year return levels of 1986-2005 annual largest daily rainfall (R_{20}, top left panel), the annual coldest temperature (TN, top right panel), non-overlapping 5-day mean rainfall ($\bar{R}^5_{20}$, middle left panel), and the annual warmest temperature (TX, middle right panel) as simulated by CMIP5 models plotted on a log scale. Rainfall extremes estimated from the reanalysis are displayed in black. The CMAP and GPCP pentad rainfall extremes are displayed by brown curves. Bottom panel: Box-and-whisker plots of simulated regionally averaged 1986-2005 R_{20} and $\bar{R}^5_{20}$. Symbols to the right of the box-and-whisker plots indicate the corresponding statistics estimated from the reanalyses and CMAP pentad dataset.

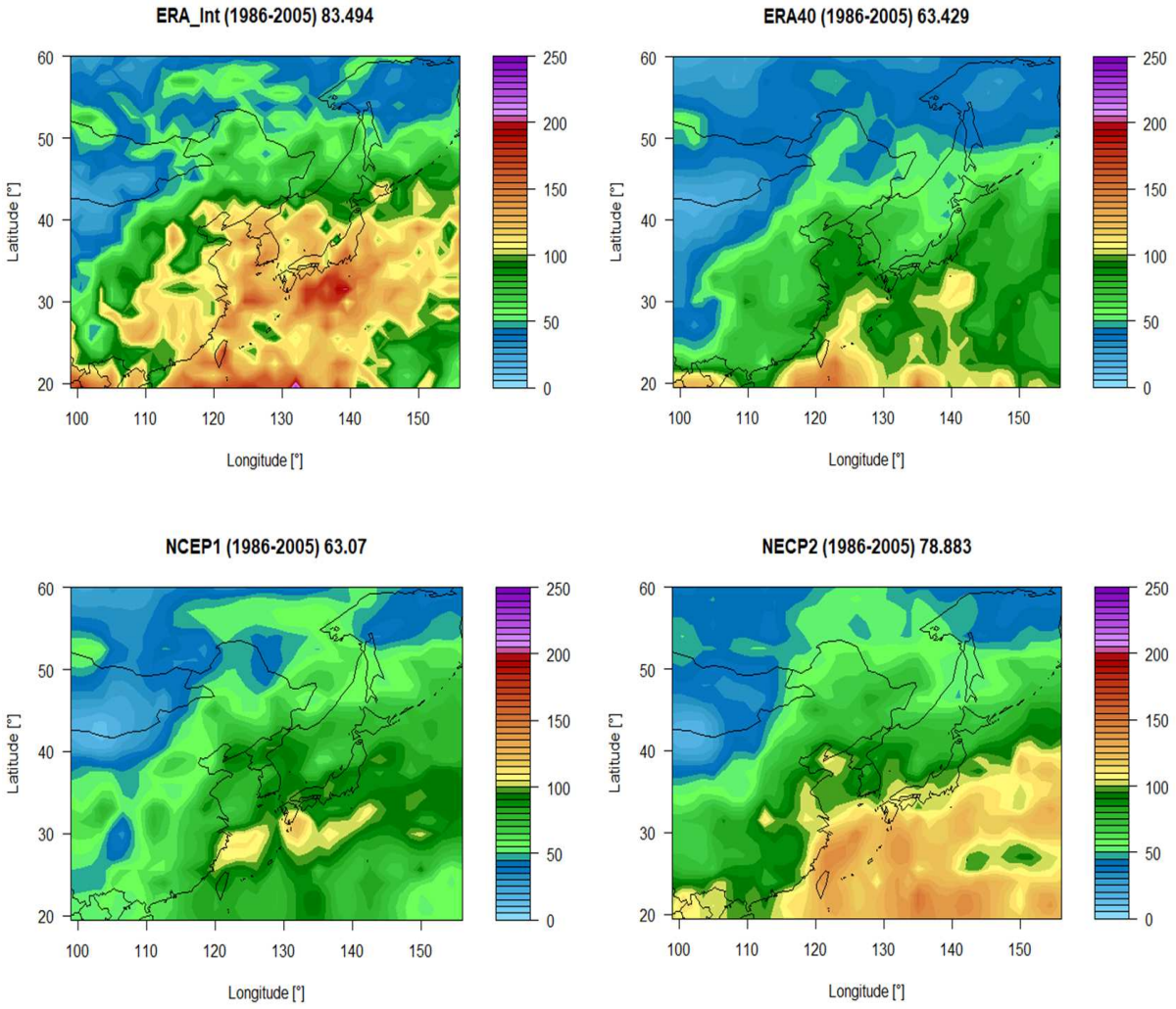

Figure S 3: Contour maps of 20-year return level of the annual largest daily rainfall for the reference period (1986–2005) obtained from 4 different reanalysis datasets (ERA-I, ERA40, NCEP1, and NCEP2).

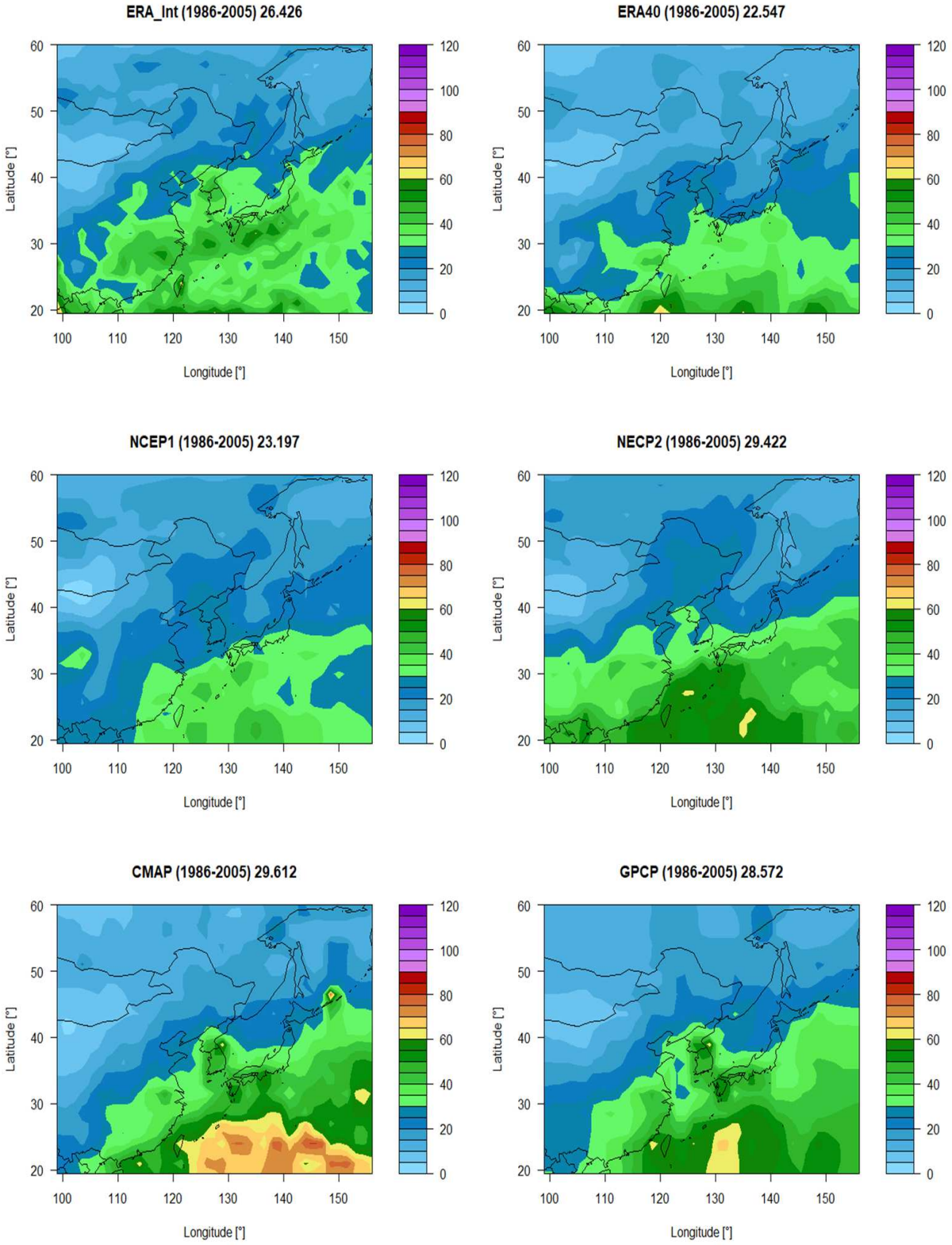

Figure S 4: Contour maps of 20-year return level of the annual largest 5-day rainfall for the reference period (1986–2005) obtained from 6 different reanalysis datasets (ERA-I, ERA40, NCEP1, NCEP2, CMAP and GPCP).

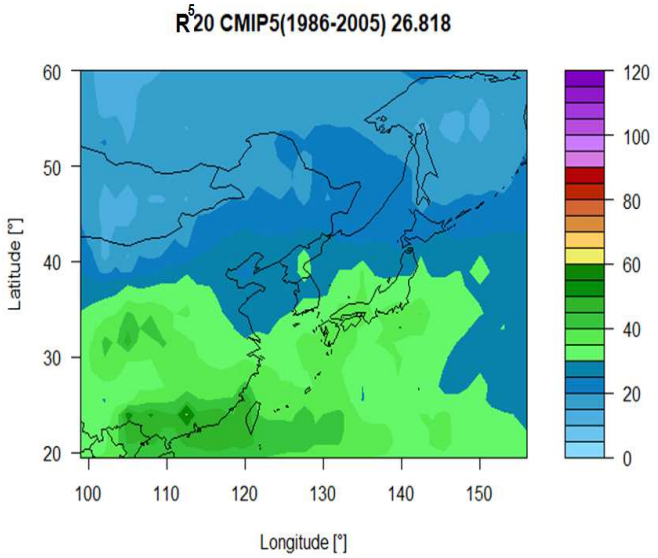

Figure S 5: Contour map of 20-year return level of the annual largest 5-day rainfall for the reference period (1986–2005) obtained from CMIP5 ensemble for the historical pentad data.

4.2 Changes in rainfall extremes

Figure S8 shows the changes of the annual mean precipitation for future three periods from CMIP5 MME relative to the period 1986-2005. Figure S9 shows the box-and-whisker plots of relative changes (%) in the regionally averaged 20-year return levels of annual extremes of daily rainfall rates (ΔR_{20}) and of regional medians of waiting times of 1986-2005 R_{20} as simulated by CMIP5 models in the three periods relative to 1986-2005 in the three RCP experiments.

References

Coles S (2001) An Introduction to Statistical Modelling of Extreme Values. Springer, New York, pp 224.

Dee DP, Uppala SM, Simmons AJ, Berrisford P, Poli P et al (2011) The ERA-Interim reanalysis: configuration and performance of the data assimilation system. Quart J R Meteor Soc 137:553–597. doi:10.1002/qj.828

Dupuis DJ, Tsao M (1998) A hybrid estimator for the generalized Pareto and extreme-value distributions. Commun Statist-Theory Meth 27:925–941. doi:10.1080/03610929808832136

Hosking JRM (1990) L-moments: analysis and estimation of distributions using linear combinations of order statistics. J Roy Statist Soc 52:105–124.

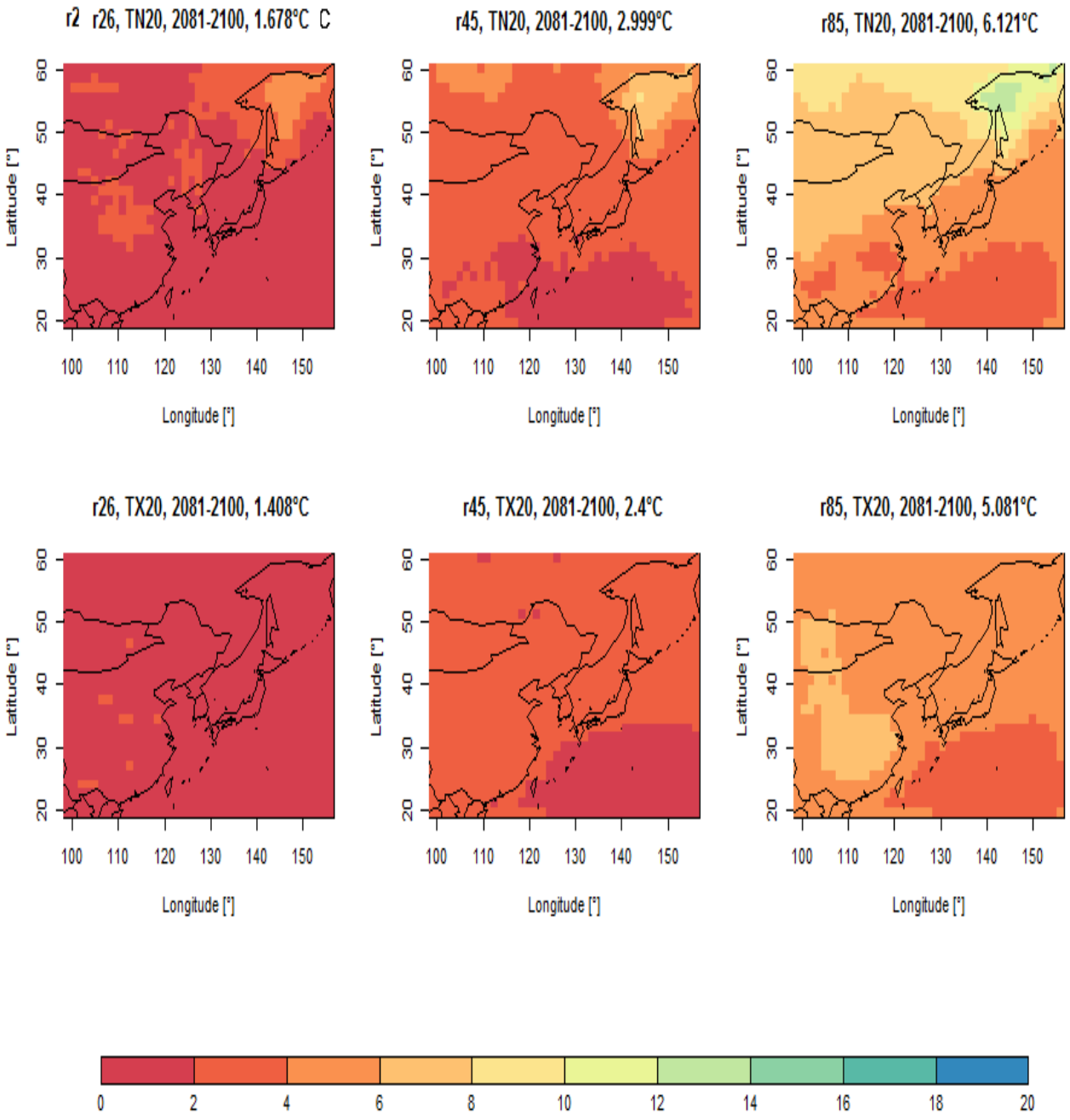

Figure S 6: Top row: CMIP5 median future relative changes (%) in 20-year return levels of annual coldest temperature TN_{20} simulated in 2081–2100 relative to 1986–2005 in RCP2.6 (left), RCP4.5 (middle), and RCP8.5 (right). Bottom row: Same as the above but for annual warmest temperature TX_{20}.

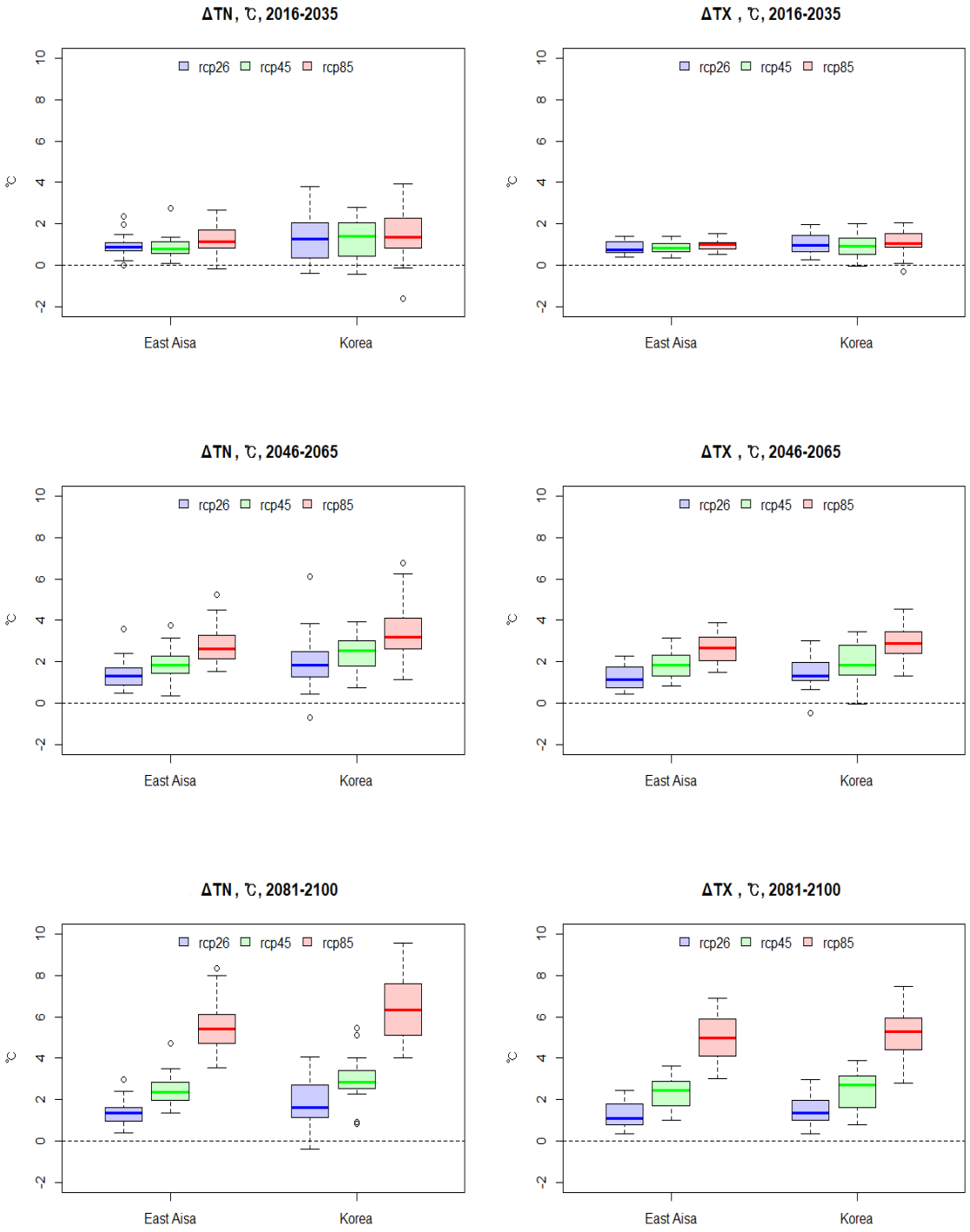

Figure S 7: Box-and-whisker plots of the future changes (°C) in averaged warm temperature extremes (TX_{20}) and cold temperature extremes (TN_{20}) as simulated by CMIP5 models in 2016-2035, 2046-2065, and 2081-2100 relative to 1986-2005.

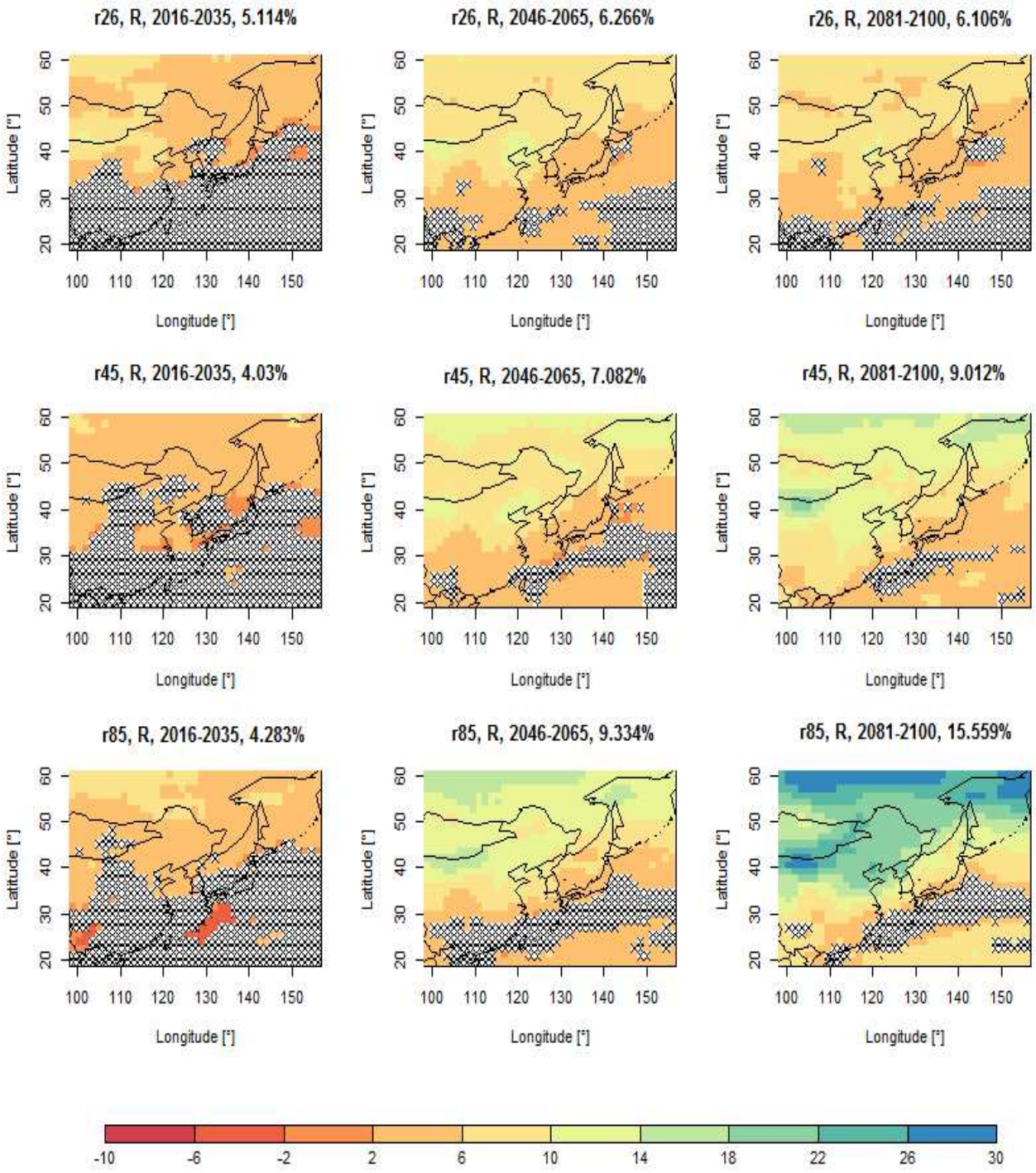

Figure S 8: CMIP5 median relative change (%) in annual mean precipitation as simulated in 2016-2035 (left column), 2046-2065 (middle column) and 2081-2100 (right column) relative to 1986-2005 in RCP2.6 (top panels), RCP4.5 (middle panels), and RCP8.5 (bottom panels). Averages of relative changes are indicated in the tiles. Changes that are not statistically significant at the 5% level are marked by cross-hatching.

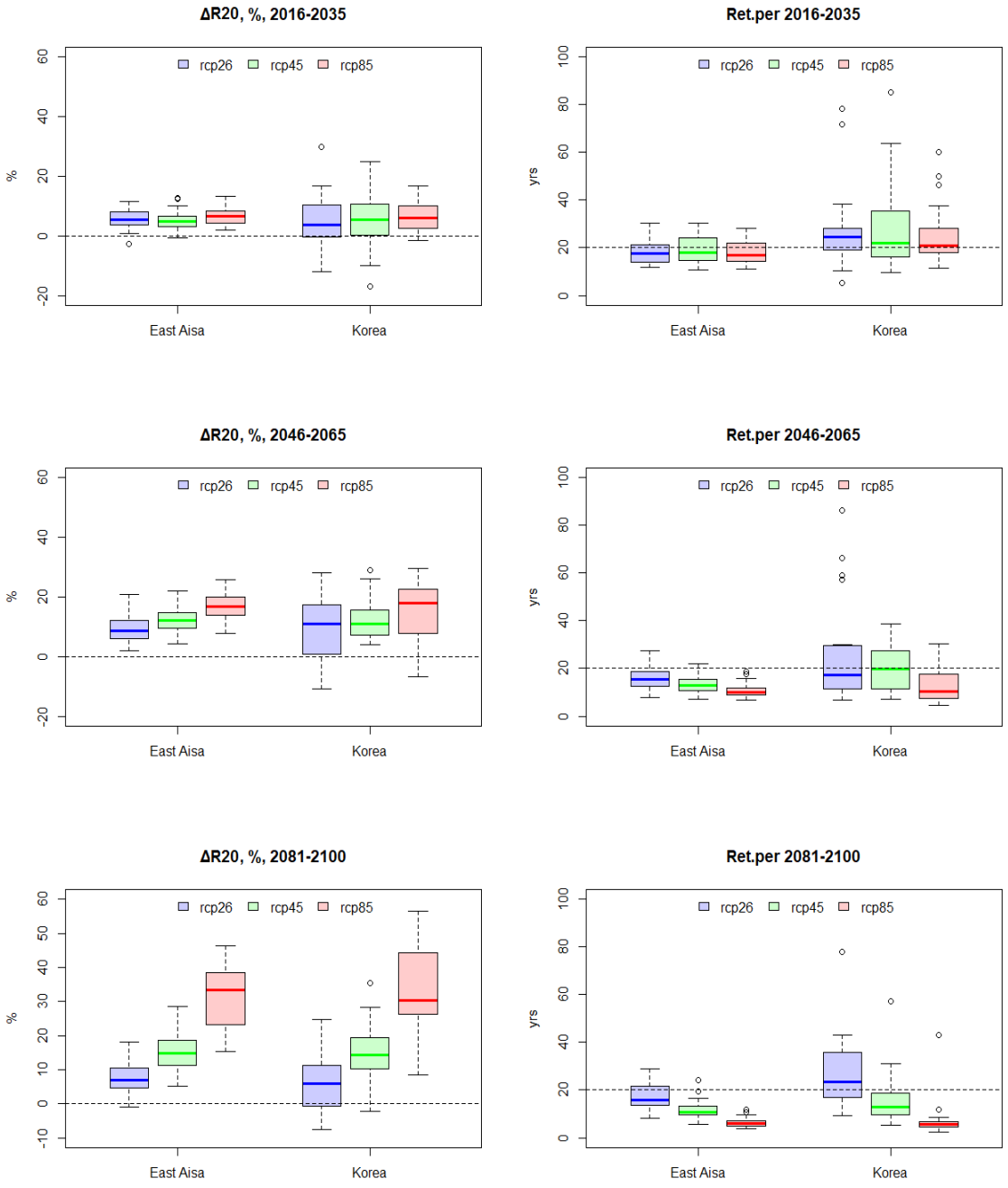

Figure S 9: Left panels: Box-and-whisker plots of relative changes (%) in the regionally averaged 20-year return levels of annual extremes of daily rainfall (ΔR_{20}) as simulated by CMIP5 models in 2016-2035, 2046-2065 and 2081-2100 relative to 1986-2005 in the RCP2.6 (blue), RCP4.5 (green) and RCP8.5 (red) experiments. The boxes indicate the central 50% inter-model range and the median. Right panels: Same as the left panels but for regional medians of the waiting times relative to R_{20} of 1986–2005.

Kalnay E, Kanamitsu M, Kistler R, Collins W, Deaven D et al (1996) The NCEP/NCAR 40-year reanalysis project. Bull Amer Meteor Soc 77:437–471

Kanamitsu M, Ebisuzaki W, Woollen J, Yang SK, Hnilo JJ et al (2002) NCE/DOE AMIP-II Reanalysis (R-2). Bull Amer Meteor Soc 83:1631–1643.

Kharin VV, Zwiers FW (2005) Estimating extremes in transient climate change simulations. J Climate 18:1156–1173.

Kharin VV, Zwiers FW, Zhang X, Hegerl GC (2007) Changes in temperature and precipitation extremes in the IPCC ensemble of global coupled model simulations. J Climate 20:1419–1444.

Kharin VV, Zwiers FW, Zhang X, Wehner M (2013) Changes in temperature and precipitation extremes in the CMIP5 ensemble. Clim Change 119:345–357.

Taylor KE (2001) Summarizing multiple aspects of model performance in a single diagram. J Geophys Res 106:7183–7192.

Uppala SM, Kallberg PW, Simmons AJ, Andrae U, Bechtold VD et al (2005) The ERA-40 re-analysis. Quart J R Meteor Soc 131:2961–3012. doi:10.1256/qj.04.176

Xie P, Arkin PA (1997) Global precipitation: a 17-year monthly analysis based on gauge observations, satellite estimates, and numerical model outputs. Bull Amer Meteor Soc 78:2539–2558

Xie P, Janowiak JE, Arkin PA, Adler R, Gruber A et al (2003) GPCP pentad precipitation analyses: An experimental dataset based on gauge observations and satellite estimates. J Climate 16:2197–2214